International Journal of Engineering

Journal Homepage: www.ije.ir

Electrolyte Temperature Dependency of Electrodeposited Nickel in Sulfate Solution on the Hardness and Corrosion Behaviors

S. Syamsuir*[a], B. Soegijono[b], S. D. Yudanto[c], B. Basori[d], M. K. Ajiriyanto[e], D. Nanto[f], F. B. Susetyo[a]

[a] *Departement of Mechanical Engineering, Universitas Negeri Jakarta, Indonesia*
[b] *Department of Geoscience, Universitas Indonesia, Indonesia*
[c] *Research Center for Metallurgy - National Research and Innovation Agency, Indonesia*
[d] *Department of Mechanical Engineering, Universitas Nasional, Indonesia*
[e] *Research Center for Nuclear Fuel Cycle and Radioactive Waste Technology - National Research and Innovation Agency, Indonesia*
[f] *Department of Physics Education, UIN Syarif Hidayatullah, Indonesia*

PAPER INFO

Paper history:
Received 13 March 2023
Received in revised form 13 May 2023
Accepted 14 May 2023

Keywords:
Ni Films
Electrodeposition
Crystallite Size
Micro-strain

ABSTRACT

The hardness and corrosion resistance of nickel (Ni) deposit on a substrate could be reached by controlling electrolyte temperature during deposition. In this research, the electrodeposition of Ni at various temperatures of electrolytes was performed. Electrodeposited Ni films using an optical digital camera, X-ray diffraction (XRD), scanning electron microscope with energy-dispersive x-ray spectroscopy (SEM-EDS), microhardness test, and potentiostat were investigated. The bright deposit occurred at 25 °C; an increase in the temperature to 40 °C leads to a change of color into semi-bright. Shifting to a higher temperature would increase the deposition rate, cathodic current efficiency, grain size, and oxygen content. The X-ray reflections in the planes (111), (200), and (220) correspond to as the Ni phase with a face center cubic (FCC) crystal structure. Decreasing crystallite size and micro-strain promoted to reach high hardness. Increasing the corrosion current density implies decreasing polarization resistance. The sample at the lowest electrolyte temperature has a better hardness, and the sample formed at 25 °C sulfate solution had less corrosion rate.

doi: *10.5829/ije.2023.36.06c.18*

NOMENCLATURE

Cor Rate	Corrosion rate (mmpy)	k	Shape factor (k=0.94)
C	Corrosion rate constant (3.27)	λ	The wavelength of the radiation source (nm)
M	Weight of the Ni atomic (g/mol)	D	The crystallite size (nm)
I_{corr}	Corrosion current density (A/cm^2)	β	Peak full width at half maximum (radians)
n	Number of Ni electrons	θ	Phase peak angle (°)
ρ	Ni density (8.908 g/cm^3)	ε	Micro-strain (%)
E_{corr}	Corrosion potential (V)	R_{ct}	Polarization resistance (Ω)

1. INTRODUCTION

Nickel (Ni) has many advantages of physical and other properties, such as better corrosion resistance and hardness [1, 2]. NiO formation on the Nickel surface could form the passive nickel layer and increase the corrosion resistance and hardness. Ni is widely used as a protective coating from corrosion attacks on automotive vehicle components and accessories such as logos, door handles, and rearview handles [3]. For those reasons, hardness and corrosion resistance properties are needed.

Numerous methods could be conducted to protect the material from corrosion attacks, such as coating, electrodeposition, hot-dip galvanizing, chemical vapor deposition (CVD), and physical vapor deposition (PVD) [4, 5]. The electrodeposition process makes Ni as

*Corresponding Author Institutional Email: syamsuir@unj.ac.id
(S. Syamsuir)

Please cite this article as: S. Syamsuir, B. Soegijono, S. D. Yudanto, B. Basori, M. K. Ajiriyanto, D. Nanto, F. B. Susetyo, Electrolyte Temperature Dependency of Electrodeposited Nickel in Sulfate Solution on the Hardness and Corrosion Behaviors, ***International Journal of Engineering, Transactions C: Aspects***, Vol. 36, No. 06, (2023), 1193-1200

protective film from corrosion attack, more promising due to being faster, cheaper, and more environmental friendly [6]. Parameters such as current density, temperature, and bath formula must be considered for better hardness and corrosion resistance.

Recently, there have been many studies on the electrodeposition of Ni to increase the hardness and corrosion resistance. Wasekar et al. [7] conducted electrodeposition by varying pulse frequency, current density, and saccharin and found saccharin significantly influences hardness. Gu et al. [8] electrodeposited Ni on a brass substrate using a choline chloride-ethylene glycol solution, producing a film's hardness of around 7.6-9.7 GPa. Furthermore, potentiodynamic polarization measurement in 3% NaCl solution showed 0.0102 mA/cm^2 of corrosion current. Yamamoto et al. [9] fabricated a Ni layer in a sulfamate bath with various current densities resulting in a hardness of around 380 HV when plating with 20 mA/cm^2. Bigos et al. [10] found Ni films hardness around 620 HV when electrodeposition in a citrate-based bath. Cheng et al. [11] observed Ni film was electrodeposited by reverse pulsed current, and varying saccharin found less grain size and corrosion current in 5 g/l saccharin addition.

The hardness and corrosion resistance could also be reached by controlled electrolyte temperature. Chung et al. [12] varied the temperature of the electrolyte solution 5, 10, 15, and 20 °C to produce a Ni film at the highest hardness at 5 °C. Jinlong et al. [13] also reported that Ni electrodeposition at 20, 50, and 80 °C temperature variations produced the lowest corrosion rates at 20 °C. Furthermore, in previous work, by varying the temperature of the electrolyte solution, 20, 30, and 50 °C found the highest hardness at 20 °C and the lowest corrosion rate at 50 °C [14].

As mentioned above, many researchers vary bath composition to reach high hardness and corrosion resistance. Varying temperatures have been conducted; other researchers also used a complex bath. This condition could raise the new problem of waste treatment before releasing it into nature.

For that reason, the electrodeposition of Ni in 0.5 M $NiSO_4$ solution without any additions and variations in temperature needs further investigation. In this research, the electrodeposition of Ni with various temperatures was performed using an electrolyte solution without additive addition.

2. EXPERIMENTAL

2. 1. Process and Materials The Ni electrodeposition process used DC power supply apparatus in 0.5 M $NiSO_4$ solution using 10mA cm^{-2} of current density. The electrodeposition was carried out in a 250 ml electrolyte plating bath at temperatures 10, 25, and 40 °C for 1 h. The sample was designated as T10, T25, and T40 for electrolyte temperatures 10, 25, and 40 °C, respectively.

Pure Ni was used as the anode, and copper alloy [14] was used for the cathode. Before the electrodeposition process, the cathode was polished sequentially using abrasive paper of #1000 up to #3000. Moreover, the cathode was cleaned with acetone before electrodeposition was performed.

2. 2. Characterization For visual appearance, the picture was captured using a digital camera. Afterwards, the captured figures were analyzed by visual appearance. The mass increment of the Ni films was found by weighing the substrate before and after electrodeposition. Moreover, a mass of the Ni films is inserted in the current efficiency and deposition rate equation. The cathodic current efficiency (CCE) and deposition rate (v) were calculated similarly by the methode as previously reported [15].

The X-ray diffraction (XRD) identified the phase and crystal structure of the films Ni with the Cu Kα radiation (Philips binary sweep). XRD data was collected from 30° to 80° with a step size of 0.020°.

Surface morphology and composition of Ni films were analyzed with FE-SEMFEI INSPECT F50 energy dispersive analysis of X-rays (EDAX) EDS analyzer.

The potentiodynamic polarization was carried out in an electrochemical workstation (Digi-Ivy DY 2311) at 30 °C. A three-electrode cell was used with a Pt as a counter electrode, an Ag/AgCl electrode as a reference electrode, and a 1 cm^2 Ni film embedded in epoxy resin as a working electrode. The potentiodynamic polarization measurement performs with a 1 mV/s scan rate in 3.5% NaCl solution.

The Tafel extrapolation methods were used to find the I_{corr} and the E_{corr}. Afterwards, the following equation was used to calculate the corrosion rate (*Cor Rate*) [16];

$$Cor\ Rate = C\frac{M \times I_{corr}}{n \times \rho} \quad (1)$$

The microhardness test was carried out with a MicroMet® 5100 series. The test was conducted with a load of 100 g for 10 s and according to the ATM E384 standard.

3. RESULTS AND DISCUSSION

3. 1. Visual Appearance Based on Figure 1, the bright deposit occurred at 25°C; an increase in the temperature to 40°C leads to a change of colour into semi-bright. A decrease in the temperature to 10°C leads to a shift in the dullness. Usually, bright deposits result in lower current densities, and dull deposits at higher current densities [17]. Furthermore, additive addition also affected the appearance quality of deposition [18].

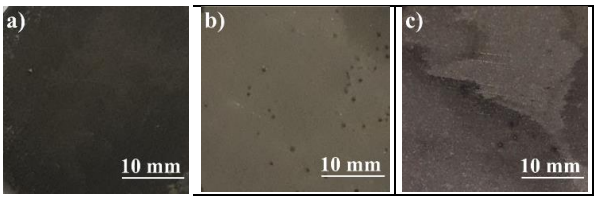

Figure 1. The visual appearance of Ni films (a) T 10, (b) T 25, and (c) T 40

3. 2. Cathodic Current Efficiency and Deposition Rate Various sample's cathodic current efficiency results can be observed in Figure 2. This behaviour indicated that the cathodic current efficiency depends strongly on temperature. Shifting to a higher temperature would affect to increase the cathodic current efficiency. Sarac and Baykul [19] found higher temperatures lead to higher cathodic current efficiency. This condition means faster Ni^{2+} ions moving in the forward direction from the anode to the cathode and promotes increasing the cathodic current efficiency as the temperature of the electrolyte solution rises. Moreover, the shift to the higher temperature affects nearly equally the deposition of Ni and hydrogen evolution [20].

Electrolyte temperature decreased when the deposition was performed, affecting the decrease of the Ni films deposition rate. A measurement result of the deposition rate of electrodeposited Ni films is shown in Figure 2. Because the deposition rate is limited by poor mass transfer conditions at low electrolyte temperatures [21]. It would influence the movement of Ni^{2+} ions from the anode to the cathode becomes slower with decreasing electrolyte temperature. Kang et al. [22] found that elevating the electrolyte temperature increased the deposition rate when electrodeposition Ni using electrolyte temperature 40 until 60 °C.

An increased in deposition rate would also influence the film thickness. Basori et al. [15] found that increased electrolyte temperature promoted the film's thickness due to increased in deposition rate. More thickness in the Ni films could influence the hardness.

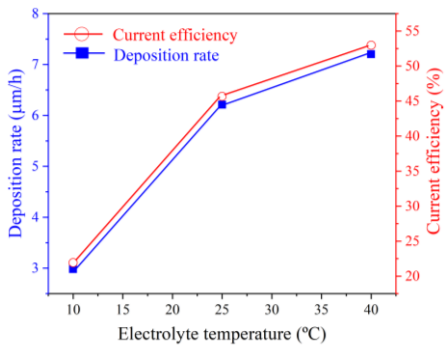

Figure 2. The cathodic current efficiency and deposition Rate of Ni films

3. 3. XRD Figure 3 illustrates the XRD pattern of electroplated Ni film samples on Cu alloy substrates at 10 °C (T10), 25 °C (T25), and 40 °C (T40). The X-ray reflections in the planes (111), (200), and (220) are defined as the Ni phase with a face centre cubic (FCC) crystal structure. According to Donegan et al. [23], Shin et al. [24] and Zhang et al. [25] these peaks are comparable to their results.

Using the JANA2006 software, the XRD pattern of Ni film samples can be very well fitted [26]. The diffraction patterns observed and the calculated results are compared in Figure 4. The calculated lattice constants of samples T10, T25, and T40 with cubic phase and fm-3m space group are 0.3522 nm, 0.3522 nm, and 0.3521 nm, respectively.

The Monshi-Scherrer and Williamson Hall Plot methods were used to analyze the effect of deposition temperature on crystallite size based on XRD patterns. Figures 5(a) and 5(b) show the Monshi-Scherrer and Williamson Hall method of the Ni film samples with a deposition temperature of 25 °C. The crystallite size can be calculated using Equation (2) based on the intercept value obtained from the ln (1/cosθ) vs ln β curve (Figure 5 (a)) [27, 28].

$$e^{ln\frac{k\lambda}{D}} = \frac{k\lambda}{D} \quad (2)$$

The crystallite size values of samples T10, T25, and T40 were 22.53 nm, 23.52 nm, and 24.54 nm, respectively. Based on the intercept values, for samples T10, T25, and T40 were -5.0471, -5.0901, and -5.1326, respectively. The Williamson Hall Plot method is used to calculate the crystallite size, which is formulated as follows [29, 30].

$$\beta.cos\theta = \frac{k\lambda}{D} + 4\varepsilon\, sin\theta \quad (3)$$

The crystallite sizes of samples T10, T25, and T40 were 27.85 nm, 36.20 nm, and 41.38 nm, respectively. This value is derived from the linear regression results of the 4.sinθ vs β.cosθ curve shown in Figure 5 (b). The micro-strain values of samples T10, T25, and T40 were 0.11%,

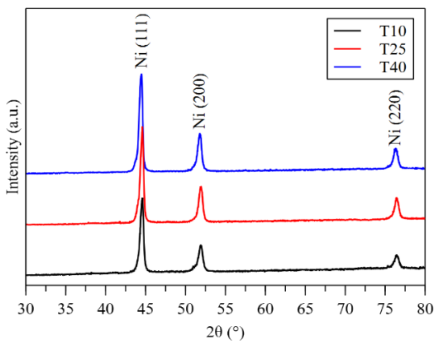

Figure 3. XRD patterns of Ni film samples with various temperature deposition

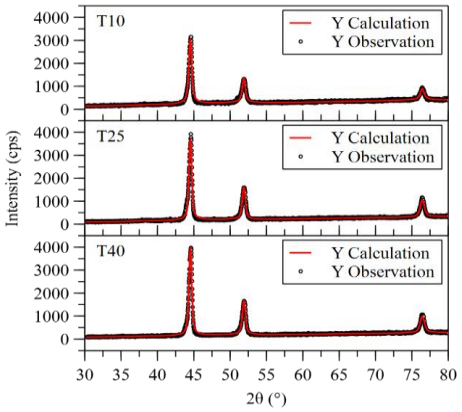

Figure 4. The observed diffraction pattern of the Ni film samples compared with the calculation results

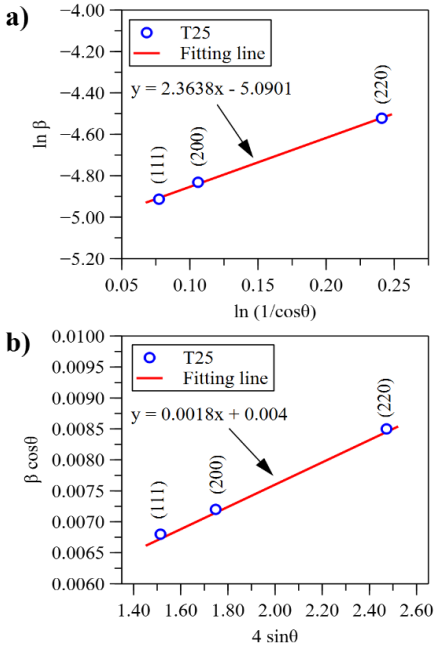

Figure 5. Calculation of the crystallite size of Ni film samples with a deposition temperature of 25 °C. (a) Monshi-Scherrer method, and (b) Williamson Hall Plot method

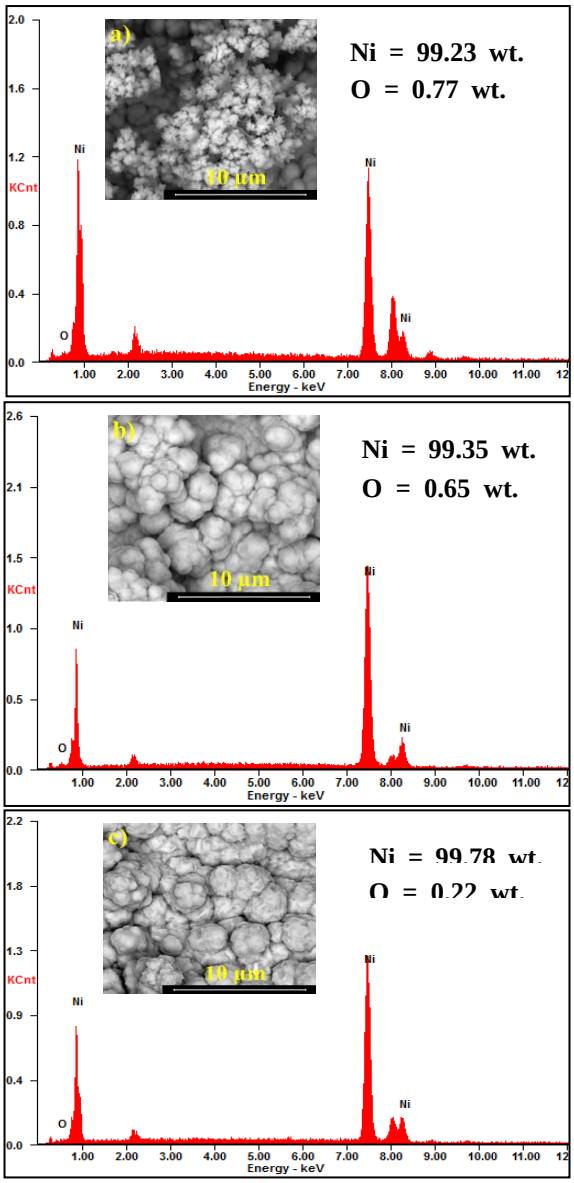

Figure 6. SEM-EDS of Ni film (a) T10, (b) T25, and (c) T40

0.18%, and 0.20%, respectively. Increasing deposition temperature causes the peaks to broaden due to lattice strain. Crystal growth of the Ni film is directly proportional to the increase in deposition temperature, according to the Monshi-Scherrer method and the Williamson Hall Plot.

3. 4. SEM-EDS The electrolyte temperature significantly influences the surface morphology of the Ni film. The SEM-EDS image (Figure 6) represents the outermost surface areas. The T10 sample shows a clear island-like structure [31]. Raising the temperature to 25 °C would change the island-like structure to a compact nodule without porosity. When the electrolyte temperature increases to 40 °C, a nodule is still seen in the surface morphology, but a little porosity is shown in the grain boundary.

Raising the temperature also influences the grain size. Compared to Figure 2, it can be seen a shift to the higher temperature on electrodeposited Ni films delivering a higher cathodic current efficiency. This behaviour means higher cathodic current efficiency produces larger grain sizes [32]. Besides current efficiency, deposition rate also contributed to grain size [33]. As seen in Figure 6, an increase in the temperature creates a larger grain size due to an increase in current efficiency and deposition rate. Lin et al. [33] reported that controlling the deposition rate leads to forming of various grain sizes.

Ni and O content is seen on the EDS examination. At high temperature, less O content is visited, and in the lowest temperature, more extensive O content is seen (Figure 6). This behaviour indicated that the oxygen content depends strongly on the temperature. Various research has been found that forming a NiO would improve corrosion resistance and hardness [34, 35]. Jabbar et al. [36] found C content in the Ni films increased by an electrolyte temperature due to the exhibit of graphene 0.2 g/l in the electrolyte solution. In contrast, within Jabbar et al. [36] research, unseen O content exists on the Ni surfaces due to probably the sample transport and storage prior to EDS characterization [14].

3. 5. Microhardness The Microhardness test result of Ni films can be seen in Figure 7. The Ni film's microhardness increases, corresponding to the electrolyte temperature decrease [22]. This behaviour perfectly agrees with Chung et al. [12] research where microhardness increases linearly when electrolyte temperature is decreased.

Compared to the XRD result, it can be seen an increase in the electrolyte temperature leads to an increase in the micro-strain. An increase in the micro-strain indicates more crystal defects that are formed and could influence the physical and mechanical properties [14, 37]. Therefore, less miro-strain would increase the hardness.

The slow deposition rate at a lower temperature promoted less crystallite size [12]. Less crystallite size could result in high hardness. Bigos et al. [10] found that shifting to a larger crystallite size decreases hardness. Martínez et al. [38] also found that reducing crystallite size would increase the hardness. This statement is in alignment with the present study.

Besides crystallite size, film thickness also contributed to the influence of the hardness. Compared to Figure 2, an increase in the electrolyte temperature can increase the deposition rate, which promotes increasing the film's thickness. Therefore, more thickness of the Ni films could increase the hardness [39].

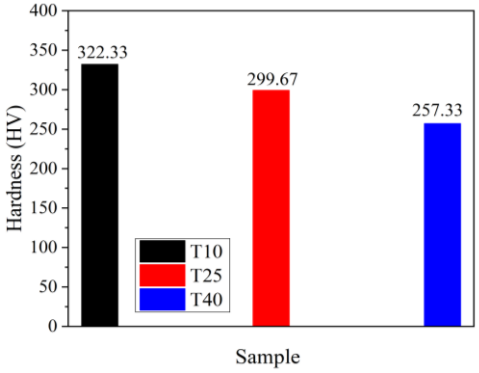

Figure 7. Microhardness test result of Ni films

The hardness of electrodeposited Ni using various bath compositions and electrolyte temperatures is summarized in Table 1.

Wasekar et al. [7] found that a saccharine in the solution significantly influences the hardness. Comparing between Figure 7 and Table 1, bath composition also contributed to high hardness besides electrolyte temperature [7]. Moreover, compared to previous work, where electrodeposited by adding H_3BO_3, resulted less hardness than present research [14].

3. 6. Potentiodynamic Polarization The potentiodynamic polarization scan results in 3.5% NaCl solution are shown in Figure 8. Shifting to high temperatures leads to producing more negative E_{corr}. This phenomenon contradicts our previous work, which could be the boric acid effect in the electrolyte solution [14]. Adding more boric acid has increased the cathodic current efficiency so that it will affect the properties of the Ni film formed. Moreover, adding boric acid also could influence strain and stress in the Ni films [40]. Increased internal stress will cause slight cracks in the Ni films [41]. Hence, those cracks would influence the E_{corr} of the Ni films.

Based on Figure 8, it can be seen that E_{corr} has a more positive value than Gu et al. [8] results. This behaviour could have different morphological results. It is seen that Gu et al. [8] had a smaller grain size than this research. Elias and Hedge [39] reported grain size would influence E_{corr}.

Based on Table 2, sample T25 has shown less corrosion rate. Moreover, the corrosion current density increases, implying decreasing polarization resistance, which means the film will be easier to corrode [42]. Furthermore, samples T10 and T40, showing active loops, indicate uniform corrosion on the film's surface (Figure 8) [43].

Compared to SEM result, compact morphology was observed in sample T25, whereas porous morphology is found in the other samples. Xu et al. [44] found porosity could influence corrosion resistance. Higher porosity

TABLE 1. Ni film's average hardness

Bath Composition (g/l)	Temp. (°C)	Hardness (HV)
$Ni(NH_2SO_3)_2$ (450), NiCl (4), and H_3BO_3 (40)	5-20	408.9-630.2 [12]
$NiSO_4$ (450) and H_3BO_3 (45)	20-50	219-259.25 [14]
$NiSO_4$ (95-110), NiCl (15-20), H_3BO_3 (30-40), surfactant (SDS) (0.4), and graphene (0.2)	15-60	220-500 [36]
$NiSO_4$ (300), NiCl (45), H_3BO_3 (40), $C_{12}H_{25}OSO_2Na$ (0.05), and $C_7H_4NO_3SNa$ (3)	50-80	510-590 [22]

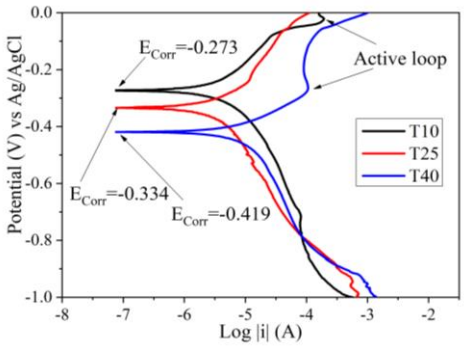

Figure 8. Potentiodynamic polarization curve of Ni films

TABLE 2. Potentiodynamic polarization of Ni films

Sample	I_{corr} (A/cm^2)	E_{corr} (V) vs Ag/AgCl	R_{ct} (Ω)	*Cor Rate* (mmpy)
T10	2.83×10^{-6}	-0.273	9088	0.0328
T25	2.49×10^{-6}	-0.334	10330	0.0280
T40	6.76×10^{-6}	-0.419	3800	0.0784

would increase the corrosion rate. Therefore sample T25 has a higher corrosion resistance than other samples.

Elias and Hedge [39] reported nodule form of the grain size would influence corrosion resistance. Based on Figure 6, nodule forms are shown in the T25 and T40 samples. Unfortunately, porosity is seen in the T40 sample. Therefore sample T25 is resulting better corrosion resistance. All conditions mentioned above can be corroborated by sample T25 has better corrosion resistance.

4. CONCLUSIONS

The characteristic of Ni films at various deposition temperature was investigated. The surface morphology of the sample looks different as the change of the electrolyte temperature. Increased electrolyte temperature is related to increase in grain size, deposition rate, cathodic current efficiency, micro-strain, and crystallite size. Moreover, decreased electrolyte temperature is related to increase in oxygen content and hardness. Sample T25 has better corrosion resistance than the other samples. Furthermore, the sample with the lowest electrolyte temperature has better hardness than the other samples.

5. ACKNOWLEDGMENTS

This work was financially supported by the Engineering Faculty of Universitas Negeri Jakarta under grant No. 065a/5.FT/PP/V/2020.

6. REFERENCES

1. Toocharoen, S., Kaewkuekool, S., and Peasura, P. "Rejuvenation heat treatment of nickel base superalloy grade GTD111 after long-term service via taguchi method for optimization." ***International Journal of Engineering, Transactions A: Basics***, Vol. 34, No. 4, (2021), 956-965. https://doi.org/10.5829/ije.2021.34.04a.22
2. Patil, V. G., Somasundaram, B., Kandaiah, S., Ramesh, M. R., and Kumar, S. "High Temperature Corrosion Behavior of High Velocity Oxy Fuel Sprayed NiCrMoFeCoAl-30%SiO2 and NiCrMoFeCoAl-30%Cr_2O_3 Composite Coatings on ASTM SA213-T22 Steel in a Coal-fired Boiler Environment." ***International Journal of Engineering, Transactions A: Basics***, Vol. 35, No. 7, (2022), 1416-1427. https://doi.org/10.5829/ije.2022.35.07a.19
3. Susetyo, F. B., Faridh, A., and Soegijono, B. "Stirring Effect on Surface Morphology, Structure, and Electrochemical Behavior of Electrodeposited Nickel Film on Copper Substrates." ***IOP Conference Series: Materials Science and Engineering***, Vol. 694, No. 1, (2019), 1-5. https://doi.org/10.1088/1757-899X/694/1/012040
4. Poursaiedi, E., and Salarvand, A. "Comparison of properties of Ti/TiN/TiCN/TiAlN Film deposited by cathodic arc physical vapor and plasma-assisted chemical vapor deposition on custom 450 steel substrates." ***International Journal of Engineering, Transactions A: Basics***, Vol. 29, No. 10, (2016), 1459-1468. https://doi.org/10.5829/idosi.ije.2016.29.10a.17
5. Moosaei, H. R., Zareei, A. R., and Salemi, N. "Elevated Temperature Performance of Concrete Reinforced with Steel, Glass, and Polypropylene Fibers and Fire-proofed with Coating." ***International Journal of Engineering, Transactions B: Applications***, Vol. 35, No. 5, (2022), 917-930. https://doi.org/10.5829/ije.2022.35.05b.08
6. Bazzaoui, M., Martins, J. I., Bazzaoui, E. A., and Albourine, A. "Environmentally friendly process for nickel electroplating of ABS." ***Applied Surface Science***, Vol. 258, No. 20, (2012), 7968-7975. https://doi.org/10.1016/j.apsusc.2012.04.146
7. Wasekar, N. P., Haridoss, P., Seshadri, S. K., and Sundararajan, G. "Influence of mode of electrodeposition , current density and saccharin on the microstructure and hardness of electrodeposited nanocrystalline nickel coatings." ***Surface & Coatings Technology***, Vol. 291, (2016), 130-140. https://doi.org/10.1016/j.surfcoat.2016.02.024
8. Gu, C. D., You, Y. H., Yu, Y. L., Qu, S. X., and Tu, J. P. "Microstructure, nanoindentation, and electrochemical properties of the nanocrystalline nickel film electrodeposited from choline chloride-ethylene glycol." ***Surface and Coatings Technology***, Vol. 205, No. 21-22, (2011), 4928-4933. https://doi.org/10.1016/j.surfcoat.2011.04.098
9. Yamamoto, T., Igawa, K., Tang, H., Chen, C. Y., Chang, T. F. M., Nagoshi, T., Kudo, O., Maeda, R., and Sone, M. "Effects of current density on mechanical properties of electroplated nickel with high speed sulfamate bath." ***Microelectronic Engineering***, Vol. 213, (2019), 18-23. https://doi.org/10.1016/j.mee.2019.04.012
10. Bigos, A., Wolowicz, M., Janusz-Skuza, M., Starowicz, Z., Szczerba, M. J., Bogucki, R., and Beltowska-Lehman, E. "Citrate-based baths for electrodeposition of nanocrystalline nickel coatings with enhanced hardness." ***Journal of Alloys and Compounds***, Vol. 850, (2021), 156857. https://doi.org/10.1016/j.jallcom.2020.156857
11. Cheng, W., Ge, W., Yang, Q., and Qu, X. "Study on the corrosion properties of nanocrystalline nickel electrodepositied by reverse pulse current." ***Applied Surface Science***, Vol. 276, (2013), 604-608. https://doi.org/10.1016/j.apsusc.2013.03.139

12. Chung, C. K., Chang, W. T., Chen, C. F., and Liao, M. W. "Effect of temperature on the evolution of diffusivity, microstructure and hardness of nanocrystalline nickel films electrodeposited at low temperatures." ***Materials Letters***, Vol. 65, No. 3, (2011), 416-419. https://doi.org/10.1016/j.matlet.2010.10.064
13. Jinlong, L., Tongxiang, L., and Chen, W. "Effect of electrodeposition temperature on grain orientation and corrosion resistance of nanocrystalline pure nickel." ***Journal of Solid State Chemistry***, Vol. 240, (2016), 109-114. https://doi.org/10.1016/j.jssc.2016.05.025
14. Susetyo, F. B., Fajrah, M. C., and Soegijono, B. "Effect of Electrolyte Temperature on Properties of Nickel Film Coated onto Copper Alloy Fabricated by Electroplating." ***e-Journal of Surface Science and Nanotechnology***, Vol. 18, (2020), 223-230. https://doi.org/10.1380/ejssnt.2020.223
15. Basori, Soegijono, B., and Susetyo, F. B. "Magnetic field exposure on electroplating process of ferromagnetic nickel ion on copper substrate." ***Journal of Physics: Conference Series***, Vol. 2377, No. 012002, (2022), 1-7. https://doi.org/10.1088/1742-6596/2377/1/012002
16. Yang, Z., Liu, X., and Tian, Y. "Fabrication of super-hydrophobic nickel film on copper substrate with improved corrosion inhibition by electrodeposition process." ***Colloids and Surfaces A: Physicochemical and Engineering Aspects***, Vol. 560, (2019), 205-212. https://doi.org/10.1016/j.colsurfa.2018.10.024
17. SEKAR, R. "Synergistic effect of additives on electrodeposition of copper from cyanide-free electrolytes and its structural and morphological characteristics." ***Transactions of Nonferrous Metals Society of China (English Edition)***, Vol. 27, No. 7, (2017), 1665-1676. https://doi.org/10.1016/S1003-6326(17)60189-4
18. Fukumoto, K., Oue, S., Kikuchi, Y., Akamatsu, S., Takasu, T., and Nakano, H. "Effect of organic additives on the electrodeposition behavior of Zn from an alkaline zincate solution and its microstructure." ***Materials Transactions***, Vol. 61, No. 3, (2020), 497-505. https://doi.org/10.2320/matertrans.MT-M2019316
19. Sarac, U., and Baykul, M. C. "Morphological and microstructural properties of two-phase Ni-Cu films electrodeposited at different electrolyte temperatures." ***Journal of Alloys and Compounds***, Vol. 552, (2013), 195-201. https://doi.org/10.1016/j.jallcom.2012.10.071
20. Kamel, M. M., Anwer, Z. M., Abdel-Salam, I. T., and Ibrahim, I. S. "Nickel electrodeposition from novel lactate bath." ***Transactions of the IMF***, Vol. 88, No. 4, (2010), 191-197. https://doi.org/10.1179/002029610X12696136822437
21. Chung, C. K., Chang, W. T., and Hung, S. T. "Electroplating of nickel films at ultra low electrolytic temperature." ***Microsystem Technologies***, Vol. 16, No. 8-9, (2010), 1353-1359. https://doi.org/10.1007/s00542-009-0955-6
22. Kang, J. X., Zhao, W. Z., and Zhang, G. F. "Influence of electrodeposition parameters on the deposition rate and microhardness of nanocrystalline Ni coatings." ***Surface and Coatings Technology***, Vol. 203, No. 13, (2009), 1815-1818. https://doi.org/10.1016/j.surfcoat.2009.01.003
23. Donegan, K. P., Godsell, J. F., Otway, D. J., Morris, M. A., Roy, S., and Holmes, J. D. "Size-tuneable synthesis of nickel nanoparticles." ***Journal of Nanoparticle Research***, Vol. 14, No. 1, (2012), 1-10. https://doi.org/10.1007/s11051-011-0670-y
24. Shin, S. M., Lee, D. W., and Wang, J. P. "Fabrication of nickel nanosized powder from LiNiO2 from spent lithium-ion battery." ***Metals***, Vol. 8, No. 1, (2018), 1-6. https://doi.org/10.3390/met8010079
25. Zhang, J., Leung, P., Qiao, F., Xing, L., Yang, C., Su, H., and Xu, Q. "Balancing the electron conduction and mass transfer: Effect of nickel foam thickness on the performance of an alkaline direct ethanol fuel cell (ADEFC) with 3D porous anode." ***International Journal of Hydrogen Energy***, Vol. 45, No. 38, (2020), 19801-19812. https://doi.org/10.1016/j.ijhydene.2020.05.119
26. Petrícek, V., Dušek, M., and Palatinus, L. "Crystallographic computing system JANA2006: General features." ***Zeitschrift fur Kristallographie***. https://doi.org/10.1515/zkri-2014-1737
27. Yudanto, S. D., Chandra, S. A., Roberto, R., Utama, D. P., Herlina, V. O., and Lusiana. "Phase and electrical properties of Ca3Co4O9 ceramic prepared by a citrate sol-gel route." ***Journal of Ceramic Processing Research***, Vol. 67, No. 2, (2022), 248-256. https://doi.org/10.31857/s0044457x22020076
28. Monshi, A., Foroughi, M. R., and Monshi, M. R. "Modified Scherrer Equation to Estimate More Accurately Nano-Crystallite Size Using XRD." ***World Journal of Nano Science and Engineering***, Vol. 02, No. 03, (2012), 154-160. https://doi.org/10.4236/wjnse.2012.23020
29. Mote, V., Purushotham, Y., and Dole, B. "Williamson-Hall analysis in estimation of lattice strain in nanometer-sized ZnO particles." ***Journal of Theoretical and Applied Physics***, Vol. 6, No. 1, (2012), 2-9. https://doi.org/10.1186/2251-7235-6-6
30. Yudanto, S. D., Dewi, Y. P., Sebayang, P., Chandra, S. A., Imaduddin, A., Kurniawan, B., and Manaf, A. "Influence of CNTs addition on structural and superconducting properties of mechanically alloyed MgB2." ***Journal of Metals, Materials and Minerals***, Vol. 30, No. 3, (2020), 9-14. https://doi.org/10.14456/jmmm.2020.32
31. Wang, Y. M., Zhao, D. D., Zhao, Y. Q., Xu, C. L., and Li, H. L. "Effect of electrodeposition temperature on the electrochemical performance of a Ni(OH) 2 electrode." ***RSC Advances***, Vol. 2, No. 3, (2012), 1074-1082. https://doi.org/10.1039/c1ra00613d
32. Wasekar, N. P., O'Mullane, A. P., and Sundararajan, G. "A new model for predicting the grain size of electrodeposited nanocrystalline nickel coatings containing sulphur, phosphorus or boron based on typical systems." ***Journal of Electroanalytical Chemistry***, Vol. 833, (2019), 198-204. https://doi.org/10.1016/j.jelechem.2018.11.057
33. Lin, Y., Pan, J., Zhou, H. F., Gao, H. J., and Li, Y. "Mechanical properties and optimal grain size distribution profile of gradient grained nickel." ***Acta Materialia***, Vol. 153, (2018), 279-289. https://doi.org/10.1016/j.actamat.2018.04.065
34. Abdallah, M., Zaafarany, I. A., Abd El Wanees, S., and Assi, R. "Breakdown of passivity of nickel electrode in sulfuric acid and its inhibition by pyridinone derivatives using the galvanostatic polarization technique." ***International Journal of Corrosion and Scale Inhibition***, Vol. 4, No. 4, (2015), 338-352. https://doi.org/10.17675/2305-6894-2015-4-4-4
35. Zhou, J., and Kong, D. "Effects of Ni addition on corrosion behaviors of laser cladded FeSiBNi coating in 3.5% NaCl solution." ***Journal of Alloys and Compounds***, Vol. 795, (2019), 416-425. https://doi.org/10.1016/j.jallcom.2019.05.012
36. Jabbar, A., Yasin, G., Khan, W. Q., Anwar, M. Y., Korai, R. M., Nizam, M. N., and Muhyodin, G. "Electrochemical deposition of nickel graphene composite coatings effect of deposition temperature on its surface morphology and corrosion resistance." ***RSC Advances***, Vol. 7, No. 49, (2017), 31100-31109. https://doi.org/10.1039/c6ra28755g
37. Susetyo, F. B., Soegijono, B., Yusmaniar, and Fajrah, M. C. "Deposition of nickel films on polycrystalline copper alloy with various current densities from watts solution." ***AIP Conference Proceedings***, Vol. 2331, (2021). https://doi.org/10.1063/5.0041640
38. Martínez, C., Briones, F., Aguilar, C., Araya, N., Iturriza, I., Machado, I., and Rojas, P. "Effect of hot pressing and hot isostatic pressing on the microstructure, hardness, and wear behavior of nickel." ***Materials Letters***, Vol. 273, (2020). https://doi.org/10.1016/j.matlet.2020.127944

39. Elias, L., and Hegde, A. C. "Effect of magnetic field on corrosion protection efficacy of Ni-W alloy coatings." ***Journal of Alloys and Compounds***, Vol. 712, (2017), 618-626. https://doi.org/10.1016/j.jallcom.2017.04.132

40. Tsuru, Y., Nomura, M., and Foulkes, F. R. "Effects of boric acid on hydrogen evolution and internal stress in films deposited from a nickel sulfamate bath." ***Journal of Applied Electrochemistry***, Vol. 32, No. 6, (2002), 629-634. https://doi.org/10.1023/A:1020130205866

41. Liu, S., Ji, R., Liu, Y., Zhang, F., Jin, H., Li, X., Zheng, Q., Lu, S., and Cai, B. "Effects of boric acid and water on the deposition of Ni/TiO2 composite coatings from deep eutectic solvent." ***Surface and Coatings Technology***, Vol. 409, (2021), 126834. https://doi.org/10.1016/j.surfcoat.2021.126834

42. Munasir, N., Triwikantoro, Zainuri, M., Bäßler, R., and Darminto. "Corrosion polarization behavior of Al-SiO2 composites in 1M and related microstructural analysis." ***International Journal of Engineering, Transactions A: Basics***, Vol. 32, No. 7, (2019), 982-990. https://doi.org/10.5829/ije.2019.32.07a.11

43. Krawczyk, B., Cook, P., Hobbs, J., and Engelberg, D. L. "Corrosion behavior of cold rolled type 316L stainless steel in HCl-containing environments." ***Corrosion***, Vol. 73, No. 11, (2017), 1346-1358.

44. Xu, W., Lu, X., Zhang, B., Liu, C., Lv, S., Yang, S., and Qu, X. "Effects of porosity on mechanical properties and corrosion resistances of PM-fabricated porous Ti-10Mo Alloy." ***Metals***, Vol. 8, No. 3, (2018). https://doi.org/10.3390/met8030188

Persian Abstract

چکیده

سختی و مقاومت به خوردگی رسوب نیکل (Ni)روی یک بستر را می توان با کنترل دمای الکترولیت در طول رسوب به دست آورد. در این تحقیق، رسوب الکتریکی نیکل در دماهای مختلف الکترولیت ها انجام شد. فیلم‌های نیکل با استفاده از دوربین دیجیتال نوری، پراش اشعه ایکس(XRD)، میکروسکوپ الکترونی روبشی با طیف‌سنجی پرتو ایکس پراکنده انرژی (SEM-EDS)، تست ریزسختی و پتانسیواستات مورد بررسی قرار گرفتند. رسوب روشن در ۲۵ درجه سانتیگراد رخ داده است. افزایش دما تا ٤٠ درجه سانتیگراد منجر به تغییر رنگ به نیمه روشن می شود. جابجایی به دمای بالاتر نرخ رسوب، راندمان جریان کاتدی، اندازه دانه و محتوای اکسیژن را افزایش می دهد. بازتاب اشعه ایکس در صفحات (۱۱۱)، (۲۰۰)، و (۲۲۰) به عنوان فاز Ni با ساختار کریستالی مکعبی مرکز صورت (FCC)مطابقت دارد. کاهش اندازه کریستالیت و ریز کرنش برای رسیدن به سختی بالا ارتقا یافته است. افزایش چگالی جریان خوردگی به معنی کاهش مقاومت پلاریزاسیون است. نمونه در پایین ترین دمای الکترولیت دارای سختی بهتری است و نمونه تشکیل شده در محلول سولفات ۲۵ درجه سانتی گراد سرعت خوردگی کمتری داشت.